

---

# Correctness Verification of Neural Networks

---

**Yichen Yang**  
MIT CSAIL  
yicheny@csail.mit.edu

**Martin Rinard**  
MIT CSAIL  
rinard@csail.mit.edu

## Abstract

We present the first verification that a neural network produces a *correct* output within a specified tolerance for *every* input of interest. We define correctness relative to a *specification* which identifies 1) a *state space* consisting of all relevant states of the world and 2) an *observation process* that produces neural network inputs from the states of the world. Tiling the state and input spaces with a finite number of tiles, obtaining ground truth bounds from the state tiles and network output bounds from the input tiles, then comparing the ground truth and network output bounds delivers an upper bound on the network output error for any input of interest. Results from a case study highlight the ability of our technique to deliver tight error bounds for all inputs of interest and show how the error bounds vary over the state and input spaces.

## 1 Introduction

Neural networks are now recognized as powerful function approximators with impressive performance across a wide range of applications. Current techniques, however, provide no *correctness guarantees* — there is currently no way to verify that a neural network provides correct outputs (within a specified tolerance) for *all* inputs of interest. The closest the field has come is robustness verification, which aims to verify if the network prediction is *stable* for all inputs in some neighborhood around a selected input point [6, 27, 22, 1, 21, 4, 23, 8]. But robustness verification does not guarantee that the output, even if stable, is actually correct — there is no specification that defines the correct output for any input except for the manually-labeled center point of each region.

We present the first *correctness verification* of neural networks — the first verification that a neural network produces a *correct* output within a specified tolerance for *every* input of interest. Neural networks are often used to predict some property of the world given an observation such as an image or audio recording. We therefore define correctness relative to a *specification* which identifies 1) a *state space* consisting of all relevant states of the world and 2) an *observation process* that produces neural network inputs from the states of the world. Then the inputs of interest are all inputs that can be observed from the state space via the observation process. We define the set of inputs of interest as the *feasible input space*. Because the quantity of interest that the network predicts is some property of the state of the world, the state defines the ground truth output (and therefore defines the correct output for each input to the neural network).

We present *Tiler*, the first algorithm for correctness verification of neural networks. Evaluating the correctness of the network on a single state is straightforward — use the observation process to obtain the possible inputs for that state, use the neural network to obtain the possible outputs, then compare the outputs to the ground truth from the state. To do correctness verification, we generalize this idea to work with *tiled* state and input spaces. We cover the state and input spaces with a finite number of *tiles*: each state tile comprises a set of states; each input tile is the image of the corresponding state tile under the observation process. The state tiles provide ground truth bounds for the corresponding input tiles. We use recently developed techniques from the robustness verification literature to obtain network output bounds for each input tile [27, 6, 22, 1, 12, 21]. A comparison of the ground truth

and output bounds delivers an error upper bound for that region of the state space. The error bounds for all the tiles jointly provide the correctness verification result.

We demonstrate how to do correctness verification using *Tiler* via a case study. Consider a world with a (idealized) fixed road and a camera that can vary its horizontal offset and viewing angle with respect to the centerline of the road. The state of the world is therefore characterized by the offset  $\delta$  and the viewing angle  $\theta$ . A neural network predicts the offset and the viewing angle of the camera, taking the image taken by the camera as input. The state space contains the ranges of  $\delta$  and  $\theta$  of interest. The observation process is the camera imaging process, which maps camera positions to images taken. This state space and the camera imaging process provide the specification: the feasible input space is the set of camera images that can be observed from all camera positions of interest; for each image, the camera positions of all the states that can produce this image give the possible ground truths. We tile the state space using a grid on  $(\delta, \theta)$ . Each state tile gives a bound on the ground truth of  $\delta$  and  $\theta$ . We then apply the observation process to project each state tile into the image space. By computing a bounding box for each resulting input tile and applying techniques from robustness verification [21], we obtain neural network output bounds for each input tile. Comparing the ground truth bounds and the network output bounds gives upper bounds on network prediction error for each tile. We are able to verify that our trained neural network provides good accuracy across the vast majority of the state space of interest. We are also able to effectively bound the *maximum* error the network will ever produce on any feasible input.

This paper makes the following contributions:

**Specification:** We show how to use state spaces and observation processes to specify the correctness of neural networks that predict properties of states given observations of the states as input.

**Verification:** We present the first algorithm for verifying that a neural network produces the correct output (up to a specified tolerance) for *every* input of interest. The algorithm can also compute tighter correctness bounds for focused regions of the state and input spaces.

**Case Study:** We apply this algorithm to the problem of predicting camera offsets and viewing angles to obtain the first correctness verification of a neural network. The verification proves that the network always produces correct outputs (within the specified tolerance) for all inputs of interest and characterizes how the correctness bounds vary across the state and input spaces.

## 2 Related Work

Motivated by the vulnerability of neural networks to adversarial attacks [15, 19], researchers have developed a range of techniques for verifying robustness — they aim to verify if the neural network prediction is stable in some neighborhood around a selected input point. [11] provides an overview of the field. A range of approaches have been explored, including layer-by-layer reachability analysis [25, 27] with abstract interpretation [6] or bounding the local Lipschitz constant [22], formulating the network as constraints and solving the resulting optimization problem [1, 12, 2, 21], solving the dual problem [4, 23, 17], and formulating and solving using SMT/SAT solvers [8, 5, 7]. In the context of control systems, [3] introduces an approach to verify state reachability and region stability of closed-loop systems with neural network controllers. [26] verifies safety by computes the reachable set of states and checks if they overlap with the unsafe states. Unlike the research presented in this paper, none of this prior research formalizes or attempts to verify that the neural network computes *correct* outputs within a specified tolerance for all inputs of interest.

Prior work on neural network testing focuses on constructing better test cases to expose problematic network behaviors. Researchers have developed approaches to build test cases that improve coverage on possible states of the neural network, for example neuron coverage [16, 20] and generalizations to multi-granular coverage [13] and MC/DC [9] inspired coverage [18]. [14] presents coverage-guided fuzzing methods for testing neural networks using the above coverage criteria. [20] generates realistic test cases by applying natural transformations (e.g. brightness change, rotation, add rain) to seed images. Unlike this prior research, which tests the neural network on only a set of input points, the research presented in this paper verifies correctness for all inputs of interest.

### 3 Correctness Verification of Neural Networks

Consider the general problem of taking an input observation  $x$  and trying to predict some quantity of interest  $y$ . It can be a regression problem (continuous  $y$ ) or a classification problem (discrete  $y$ ). Some neural network model is trained for this task. We denote its function by  $f : \mathcal{X} \rightarrow \mathcal{Y}$ , where  $\mathcal{X}$  is the space of all possible inputs to the neural network and  $\mathcal{Y}$  is the space of all possible outputs. Behind the input observation  $x$  there is some state of the world  $s$ . Denote  $\mathcal{S}$  as the space of all states of the world that we want to verify. For each state of the world, a set of possible inputs can be observed. We denote this *observation process* using a mapping  $g : \mathcal{S} \rightarrow \mathcal{P}(\tilde{\mathcal{X}})$ , where  $g(s)$  is the set of inputs that can be observed from  $s$ . Here  $\mathcal{P}(\cdot)$  is the power set, and  $\tilde{\mathcal{X}} \subseteq \mathcal{X}$  is the *feasible input space*, the part of input space that may be observed from the *state space*  $\mathcal{S}$ . Concretely,  $\tilde{\mathcal{X}} = \{x | \exists s \in \mathcal{S}, x \in g(s)\}$ .

The quantity of interest  $y$  is some aspect of the state of the world. We denote the ground truth of  $y$  using a function  $\lambda : \mathcal{S} \rightarrow \mathcal{Y}$ . This specifies the ground truth for each input, which we denote as a mapping  $\hat{f} : \tilde{\mathcal{X}} \rightarrow \mathcal{P}(\mathcal{Y})$ .  $\hat{f}(x)$  is the set of possible ground truth values of  $y$  for a given  $x$ :

$$\hat{f}(x) = \{y | \exists s \in \mathcal{S}, y = \lambda(s), x \in g(s)\}. \quad (1)$$

The feasible input space  $\tilde{\mathcal{X}}$  and the ground truth mapping  $\hat{f}$  together form a *specification*. In general, we cannot compute and represent  $\tilde{\mathcal{X}}$  and  $\hat{f}$  directly — indeed, the purpose of the neural network is to compute an approximation to this ground truth  $\hat{f}$  which is otherwise not available given only the input  $x$ .  $\tilde{\mathcal{X}}$  and  $\hat{f}$  are instead determined implicitly by  $\mathcal{S}$ ,  $g$ , and  $\lambda$ .

The error of the neural network is then characterized by the difference between  $f$  and  $\hat{f}$ . Concretely, the maximum possible error at a given input  $x \in \tilde{\mathcal{X}}$  is:

$$e(x) = \max_{y \in \hat{f}(x)} d(f(x), y), \quad (2)$$

where  $d(\cdot, \cdot)$  is some measurement on the size of the error between two values of the quantity of interest. For regression, we consider the absolute value of the difference  $d(y_1, y_2) = |y_1 - y_2|$ .<sup>1</sup> For classification, we consider a binary error measurement  $d(y_1, y_2) = \mathbb{1}_{y_1 \neq y_2}$  (indicator function), i.e. the error is 0 if the prediction is correct, 1 if the prediction is incorrect.

The goal of correctness verification is to compute upper bounds on network prediction errors with respect to the specification. We formulate the problem of correctness verification formally here:

**Problem formulation of correctness verification:** Given a trained neural network  $f$  and a specification  $(\tilde{\mathcal{X}}, \hat{f})$  determined implicitly by  $\mathcal{S}$ ,  $g$ , and  $\lambda$ , compute upper bounds on error  $e(x)$  for any feasible input  $x \in \tilde{\mathcal{X}}$ .

### 4 Tiler

We next present *Tiler*, an algorithm for correctness verification of neural networks. We present here the algorithm for regression settings, with sufficient conditions for the resulting error bounds to be sound. The algorithm for classification settings is similar (see Appendix B).

The first step is to use the state space  $\mathcal{S}$  to tile the feasible input space:

**Step 1:** Divide the state space  $\mathcal{S}$  into local regions  $\{\mathcal{S}_i\}$  such that  $\cup_i \mathcal{S}_i = \mathcal{S}$ .

The image of each  $\mathcal{S}_i$  under  $g$  is a *tile* on the input space:  $\mathcal{X}_i = \{x | x \in g(s), s \in \mathcal{S}_i\}$ . The resulting tiles  $\{\mathcal{X}_i\}$  satisfy the following condition:

*Condition 4.1.*  $\tilde{\mathcal{X}} \subseteq \cup_i \mathcal{X}_i$ .

The second step is to compute a ground truth bound for each input tile  $\mathcal{X}_i$ , specifically by computing the ground truth bound for the corresponding  $\mathcal{S}_i$  under the ground truth function  $\lambda$ :

<sup>1</sup>For clarity, we formulate the problem with a one-dimensional quantity of interest. Extending to multidimensional output (multiple quantities of interest) is straightforward: we treat the prediction of each output dimension as using a separate neural network, all of which are the same except the final output layer.

**Step 2:** For each  $\mathcal{S}_i$ , compute the ground truth bound as an interval  $[l_i, u_i]$ , such that  $\forall s \in \mathcal{S}_i, l_i \leq \lambda(s) \leq u_i$ .

We use this ground truth bound  $[l_i, u_i]$  for tile  $\mathcal{X}_i$ . The bounds computed this way satisfy the following condition, which (intuitively) states that the possible ground truth values for an input point must be covered jointly by the ground truth bounds of all the input tiles that contain this point:

*Condition 4.2(a).* For any  $x \in \tilde{\mathcal{X}}, \forall y \in \hat{f}(x), \exists \mathcal{X}_i$  such that  $x \in \mathcal{X}_i$  and  $l_i \leq y \leq u_i$ .

Previous research has produced a variety of methods that bound the neural network output over given input region. Examples include layer-by-layer reachability analysis [27, 6, 22] and formulating constrained optimization problems [1, 12, 21]. Each method typically works for certain classes of networks (e.g. piece-wise linear networks) and certain classes of input regions (e.g. polytopes). For each input tile  $\mathcal{X}_i$ , we therefore introduce a bounding box  $\mathcal{B}_i$  that 1) includes  $\mathcal{X}_i$  and 2) is supported by the solving method:

**Step 3:** Using  $\mathcal{S}_i$  and  $g$ , compute a bounding box  $\mathcal{B}_i$  for each tile  $\mathcal{X}_i = \{x | x \in g(s), s \in \mathcal{S}_i\}$ .

The bounding boxes  $\mathcal{B}_i$ 's must satisfy the following condition:

*Condition 4.3.*  $\forall i, \mathcal{X}_i \subseteq \mathcal{B}_i$ .

We then solve the neural network output range for each bounding box:

**Step 4:** Given  $f$  and bounding boxes  $\{\mathcal{B}_i\}$ , use an appropriate solver to solve for the network output ranges  $\{[l'_i, u'_i]\}$ .

The neural network has a single output entry for each quantity of interest. Denote the value of the output entry as  $o(x)$ ,  $f(x) = o(x)$ . The network output bounds  $(l'_i, u'_i)$  returned by the solver must satisfy the following condition:

*Condition 4.4(a)*  $\forall x \in \mathcal{B}_i, l'_i \leq o(x) \leq u'_i$ .

With the ground truth bounds and network output bounds, we can now compute the error bounds:

**Step 5:** For each tile, use the ground truth bound  $(l_i, u_i)$  and network output bound  $(l'_i, u'_i)$  to compute the error bound  $e_i$ :

$$e_i = \max(u'_i - l_i, u_i - l'_i). \quad (3)$$

$e_i$  gives the upper bound on prediction error when the state of the world  $s$  is in  $\mathcal{S}_i$ . This is because  $(l_i, u_i)$  covers the ground truth values in  $\mathcal{S}_i$ , and  $(l'_i, u'_i)$  covers the possible network outputs for all inputs that can be generated from  $\mathcal{S}_i$ . From these error bounds  $\{e_i\}$ , we compute a global error bound:

$$e_{\text{global}} = \max_i e_i. \quad (4)$$

We can also compute a local error bound for any feasible input  $x \in \tilde{\mathcal{X}}$ :

$$e_{\text{local}}(x) = \max_{\{i | x \in \mathcal{B}_i\}} e_i. \quad (5)$$

Note that  $\max_{\{i | x \in \mathcal{X}_i\}} e_i$  provides a tighter local error bound. But since it is generally much easier to check containment of  $x$  in  $\mathcal{B}_i$ 's than in  $\mathcal{X}_i$ 's, we adopt the current formulation.

We establish the soundness of the error bounds obtained from *Tiler* below.

**Theorem 1** (Local error bound for regression). *Given that Condition 4.1, 4.2(a), 4.3, and 4.4(a) are satisfied, then  $\forall x \in \tilde{\mathcal{X}}, e(x) \leq e_{\text{local}}(x)$ , where  $e(x)$  is defined in Equation 2 and  $e_{\text{local}}(x)$  is computed from Equation 3 and 5.*

**Theorem 2** (Global error bound for regression). *Given that Condition 4.1, 4.2(a), 4.3, and 4.4(a) are satisfied, then  $\forall x \in \tilde{\mathcal{X}}, e(x) \leq e_{\text{global}}$ , where  $e(x)$  is defined in Equation 2 and  $e_{\text{global}}$  is computed from Equation 3 and 4.*

Algorithm 1 formally presents the *Tiler* algorithm (for regression). The implementations of `DIVIDESTATESPACE`, `GETGROUNDTRUTHBOUND`, and `GETBOUNDINGBOX` are problem dependent. The choice of `SOLVER` needs to be compatible with  $\mathcal{B}_i$  and  $f$ . Conditions 4.1 to 4.4 specify the sufficient conditions for the returned results from these four methods such that the guarantees obtained are sound.

---

**Algorithm 1** Tiler (for regression)

---

**Input:**  $\mathcal{S}, g, \lambda, f$ **Output:**  $e_{\text{global}}, \{e_i\}, \{\mathcal{B}_i\}$ 

```

1: procedure TILER( $\mathcal{S}, g, \lambda, f$ )
2:    $\{\mathcal{S}_i\} \leftarrow \text{DIVIDESTATESPACE}(\mathcal{S})$  ▷ Step 1
3:   for each  $\mathcal{S}_i$  do
4:      $(l_i, u_i) \leftarrow \text{GETGROUNDTRUTHBOUND}(\mathcal{S}_i, \lambda)$  ▷ Step 2
5:      $\mathcal{B}_i \leftarrow \text{GETBOUNDINGBOX}(\mathcal{S}_i, g)$  ▷ Step 3
6:      $(l'_i, u'_i) \leftarrow \text{SOLVER}(f, \mathcal{B}_i)$  ▷ Step 4
7:      $e_i \leftarrow \max(u'_i - l_i, u_i - l'_i)$  ▷ Step 5
8:   end for
9:    $e_{\text{global}} \leftarrow \max(\{e_i\})$  ▷ Step 5
10:  return  $e_{\text{global}}, \{e_i\}, \{\mathcal{B}_i\}$  ▷  $\{e_i\}, \{\mathcal{B}_i\}$  can be used later to compute  $e_{\text{local}}(x)$ 
11: end procedure

```

---

Table 1: Scene parameters

| Parameter | Description       | Value | Parameter | Description            | Value |
|-----------|-------------------|-------|-----------|------------------------|-------|
| $x_1$     | Road width        | 50.0  | $i_1$     | Intensity (side line)  | 1.0   |
| $x_2$     | Line width        | 4.0   | $i_2$     | Intensity (centerline) | 0.7   |
| $x_3$     | Ramp half width   | 1.0   | $i_3$     | Intensity (road)       | 0.3   |
| $z_c$     | Camera height     | 20.0  | $i_4$     | Intensity (sky)        | 0.0   |
| $f$       | Focal length      | 1.0   | $n$       | Pixel number           | 32    |
| $d$       | Pixel side length | 0.16  |           |                        |       |

The complexity of this algorithm is determined by the number of tiles, which scales with the dimension of the state space  $\mathcal{S}$ . Because the computations for each tile are independent, our *Tiler* implementation executes these computations using parallelism.

## 5 Case Study: Position Measurement from Road Scene

We next present a case study where we use *Tiler* to verify the correctness of a neural network that estimates the position of a camera with respect to a road.

### 5.1 Problem Set-up

Consider a world containing a road with a centerline, two side lines, and a camera taking images of the road. The camera is positioned at a fixed height above the road, but can vary its horizontal offset and viewing angle with respect to the centerline of the road. Figure 1a presents a schematic of the scene. For clarity, we describe the scene in a Cartesian coordinate system. Treating 1 length unit as roughly 5 centimeters will give a realistic scale. The scene contains a road in the  $xy$ -plane, extending along the  $y$ -axis. A schematic view of the road down along the  $z$ -axis is shown in Figure 2a. The road contains a centerline and two side lines, each with width  $x_2 = 4.0$ . The width of the road (per lane) is  $x_1 = 50.0$ , measuring from the center of the centerline to the center of each side line. Each point in the scene is associated with an intensity value in  $[0.0, 1.0]$  grayscale. The intensity of the side lines is  $i_1 = 1.0$ , centerline  $i_2 = 0.7$ , road  $i_3 = 0.3$ , and sky  $i_4 = 0.0$ . The intensity adopts a ramp change at each boundary between the lines and the road. The half width of the ramp is  $x_3 = 1.0$ .

The schematic of the camera is shown in Figure 2b. The camera’s height above the road is fixed at  $z_c = 20.0$ . The focal length  $f = 1.0$ . The image plane is divided into  $32 \times 32$  pixels, with pixel side length  $d = 0.16$ . Table 1 summarizes all the scene parameters described above.

The state of the world  $s$  is characterized by the offset  $\delta$  and angle  $\theta$  of the camera position. We therefore label the states as  $s_{\delta, \theta}$ . In this problem, we consider the camera position between the range  $\delta \in [-40, 40]$  (length unit of the scene) and  $\theta \in [-60^\circ, 60^\circ]$ . This gives the state space  $\mathcal{S} = \{s_{\delta, \theta} | \delta \in [-40, 40], \theta \in [-60^\circ, 60^\circ]\}$ .

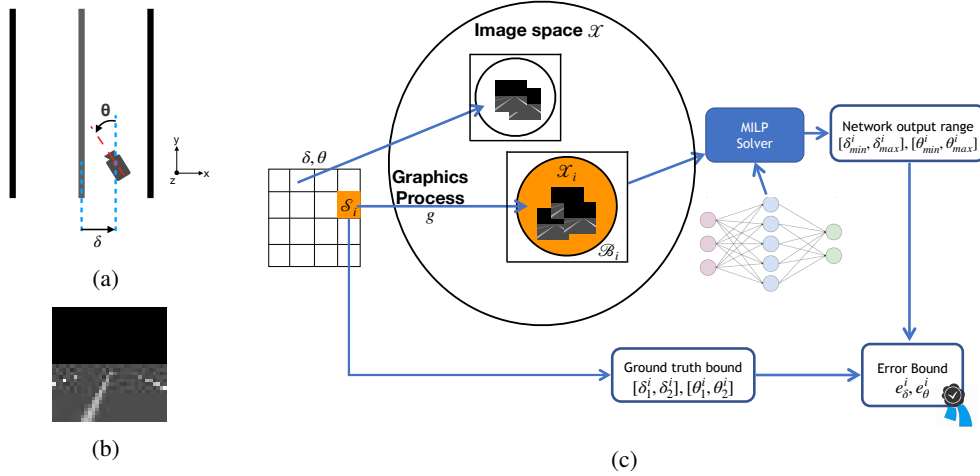


Figure 1: (a) Schematic of the scene. (b) Example image taken by the camera. (c) Schematics of *Tiler* applied on the road scene case.

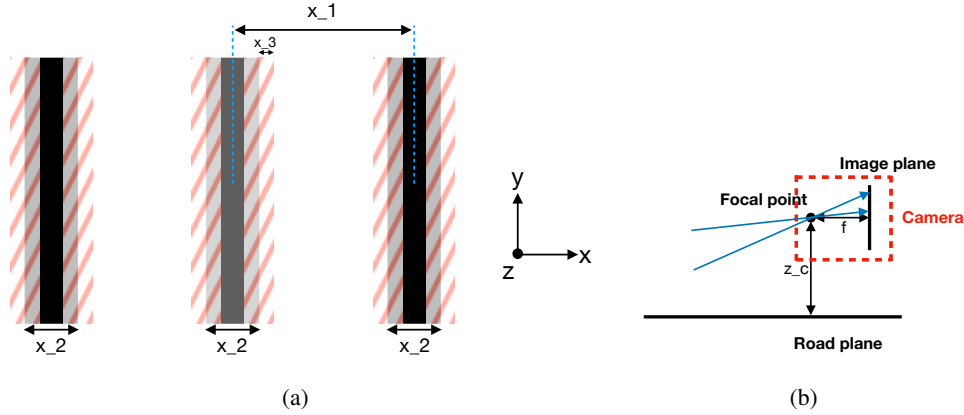


Figure 2: (a) Schematic of the top view of the road. (b) Schematic of the camera.

The input  $x$  to the neural network is the image taken by the camera. The observation process  $g$  is the camera imaging process. The camera imaging process we use can be viewed as an one-step ray tracing: the intensity value of each pixel is determined by shooting a ray from the center of that pixel through the focal point, then taking the intensity of the intersection point between the ray and the scene. In this example scene, the intersection points for the top half of the pixels are in the sky (intensity 0.0). The intersection points for the lower half of the pixels are on the  $xy$ -plane. The position of the intersection point (in the world coordinates) can be computed using a transformation from the pixel coordinates in homogeneous coordinate systems:

$$\tilde{X}_W^{(i,j)} = T_{FW} \cdot P_p \cdot R_{CF} \cdot P_{PC} \cdot \begin{bmatrix} i \\ j \\ 1 \end{bmatrix} \quad (6)$$

$P_{PC}$  is the transformation from pixel coordinates to camera coordinates. Camera coordinates have the origin at the focal point, and axes aligned with the orientation of the camera. We define the focal coordinates to have the origin also at the focal point, but with axes aligned with the world coordinates (the coordinate system used to describe the scene).  $R_{CF}$  is the rotation matrix that transforms from camera coordinates to focal coordinates.  $P_p$  represents the projection to the road plane through the

focal point, in the focal coordinates. Finally,  $T_{FW}$  is the translation matrix that transforms from the focal coordinates to the world coordinates. The transformation matrices are given below:<sup>2</sup>

$$T_{FW} = \begin{bmatrix} 1 & 0 & 0 & \delta \\ 0 & 1 & 0 & 0 \\ 0 & 0 & 1 & z_c \\ 0 & 0 & 0 & 1 \end{bmatrix}, P_P = \begin{bmatrix} -z_c & 0 & 0 & 0 \\ 0 & -z_c & 0 & 0 \\ 0 & 0 & -z_c & 0 \\ 0 & 0 & 1 & 0 \end{bmatrix}$$

$$R_{CF} = \begin{bmatrix} \cos \theta & -\sin \theta & 0 & 0 \\ \sin \theta & \cos \theta & 0 & 0 \\ 0 & 0 & 1 & 0 \\ 0 & 0 & 0 & 1 \end{bmatrix}, P_{PC} = \begin{bmatrix} 0 & d & \frac{d}{2} - \frac{nd}{2} \\ 0 & 0 & f \\ -d & 0 & -(\frac{d}{2} - \frac{nd}{2}) \\ 0 & 0 & 1 \end{bmatrix}$$

The variables are defined as in Table 1, with  $\delta$  and  $\theta$  being the offset and angle of the camera. After the intensity values of the pixels are determined, they are scaled and quantized to the range  $[0, 255]$ . The resulting input images  $x$ 's are  $32 \times 32$  gray scale images with intensities in  $[0, 255]$ . Figure 1b presents an example image. The feasible input space  $\tilde{\mathcal{X}}$  is the set of all images that can be taken with  $\delta \in [-40, 40]$  and  $\theta \in [-60^\circ, 60^\circ]$ .

The quantity of interest  $y$  is the camera position  $(\delta, \theta)$ . The ground truth function  $\lambda$  is simply  $\lambda(s_{\delta, \theta}) = (\delta, \theta)$ . For the neural network, we use the same ConvNet architecture as CNN<sub>A</sub> in [21] and the *small* network in [24]. It has 2 convolutional layers (size  $4 \times 4$ , stride 2) with 16 and 32 filters respectively, followed by a fully connected layer with 100 units. All the activation functions are ReLUs. The output layer is a linear layer with 2 output nodes, corresponding to the predictions of  $\delta$  and  $\theta$ . The network is trained on 130k images and validated on 1000 images generated from our imaging process. The camera positions of the training and validation images are sampled uniformly from the range  $\delta \in [-50, 50]$  and  $\theta \in [-70^\circ, 70^\circ]$ . The network is trained with an  $l_1$ -loss function, using *Adam* [10] (see Appendix C for more training details).

For error analysis, we treat the predictions of  $\delta$  and  $\theta$  separately. The goal is to find upper bounds on the prediction errors  $e_\delta(x)$  and  $e_\theta(x)$  for any feasible input  $x \in \tilde{\mathcal{X}}$ .

## 5.2 Tiler

Figure 1c presents a schematic of how we apply *Tiler* to this problem. Tiles are constructed by dividing  $\mathcal{S}$  on  $(\delta, \theta)$  into a grid of equal-sized rectangles with length  $a$  and width  $b$ . Each cell in the grid is then  $\mathcal{S}_i = \{s_{\delta, \theta} | \delta \in [\delta_1^i, \delta_2^i], \theta \in [\theta_1^i, \theta_2^i]\}$ , with  $\delta_2^i - \delta_1^i = a$  and  $\theta_2^i - \theta_1^i = b$ . Each tile  $\mathcal{X}_i$  is the set of images that can be observed from  $\mathcal{S}_i$ . The ground truth bounds can be naturally obtained from  $\mathcal{S}_i$ : for  $\delta$ ,  $l_i = \delta_1^i$  and  $u_i = \delta_2^i$ ; for  $\theta$ ,  $l_i = \theta_1^i$  and  $u_i = \theta_2^i$ .

We next encapsulate each tile  $\mathcal{X}_i$  with an  $l_\infty$ -norm ball  $\mathcal{B}_i$  by computing, for each pixel, the range of possible values it can take within the tile. A tile in this example corresponds to images taken with camera position in a local range  $\delta \in [\delta_1, \delta_2]$ ,  $\theta \in [\theta_1, \theta_2]$ . For pixels in the upper half of the image, their values will always be the intensity of the sky. For each pixel in the lower half of the image, if we trace the intersection point between the projection ray of this pixel and the road plane, it will sweep over a closed region as the camera position varies in the  $\delta$ - $\theta$  cell. The range of possible values for that pixel is then determined by the range of intensities in that region. In this example, there is an efficient way of computing the range of intensities in the region of sweep. Since the intensities on the road plane only vary with  $x$ , it suffices to find the span on  $x$  for the region. The extrema on  $x$  can only be achieved at: 1) the four corners of the  $\delta$ - $\theta$  cell; 2) the points on the two edges  $\delta = \delta_1$  and  $\delta = \delta_2$  where  $\theta$  makes the ray of that pixel perpendicular to the  $y$  axis (if that  $\theta$  is contained in  $[\theta_1, \theta_2]$ ). Therefore, by computing the location of these critical points, we can obtain the range of  $x$ . We can then obtain the range of intensities covered in the region of sweep, which will give the range of pixel values. The resulting  $\mathcal{B}_i$  is an  $l_\infty$ -norm ball in the image space covering  $\mathcal{X}_i$ , represented by  $32 \times 32$  pixel-wise ranges.

<sup>2</sup>Note that for this imaging process, flipping the image on the image plane to the correct orientation (originally upside-down) is equivalent to taking the image on a virtual image plane that is in front of the focal point by the focal length, by shooting rays from the focal point through the (virtual) pixel centers. We compute the intersection points from the pixel coordinates on the virtual image plane.

To solve the range of outputs of the ConvNet for inputs in the  $l_\infty$ -norm ball, we adopt the approach from [21]. They formulate the robustness verification problem as mixed integer linear program (MILP), by expressing the network computations and input constraints as linear or integer constraints. Presolving on ReLU stability and progressive bound tightening are used to improve efficiency. We adopt the same formulation but change the MILP objectives. For each  $l_\infty$ -norm ball, we solve 4 optimization problems: maximizing and minimizing the output entry for  $\delta$ , and another two for  $\theta$ . To speed up solving, we reuse the results from presolving across the 4 optimization problems of the same tile (they share the same input constraints and thus the same bounds on the internal variables of the network). Denote the optimized objectives we obtain as  $\delta_{min}^i, \delta_{max}^i, \theta_{min}^i, \theta_{max}^i$ .

We then use Equation 3 to compute the error bounds for each tile:  $e_\delta^i = \max(\delta_{max}^i - \delta_1^i, \delta_2^i - \delta_{min}^i)$ ,  $e_\theta^i = \max(\theta_{max}^i - \theta_1^i, \theta_2^i - \theta_{min}^i)$ .  $e_\delta^i$  and  $e_\theta^i$  give upper bounds on prediction error when the state of the world  $s$  is in cell  $S_i$ . These error bounds can later be used to compute global and local error bounds as in Equation 4 and 5.

### 5.3 Experimental Results

We run *Tiler* with a cell size of 0.1 (the side length of each cell in the  $(\delta, \theta)$  grid is  $a = b = 0.1$ ). The step that takes the majority of time is the optimization solver. With parallelism, the optimization step takes about 15 hours running on 40 CPUs@3.00 GHz, solving  $960000 \times 4$  MILP problems.

**Global error bound:** We compute global error bounds by taking the maximum of  $e_\delta^i$  and  $e_\theta^i$  over all tiles. The global error bound for  $\delta$  is 12.66, which is 15.8% of the measurement range (80 length units for  $\delta$ ); for  $\theta$  is  $7.13^\circ$  (5.94% of the  $120^\circ$  measurement range). We therefore successfully verify the correctness of the network with these tolerances for all feasible inputs.

**Error bound landscape:** We present the visualizations of the error bound landscape by plotting the error bounds of each tile as heatmaps over the  $(\delta, \theta)$  space. Figures 3a and 3d present the resulting heatmaps for  $e_\delta^i$  and  $e_\theta^i$ , respectively. To further inspect the distribution of the error bounds, we compute the percentage of the state space  $\mathcal{S}$  (measured on the  $(\delta, \theta)$  grid) that has error bounds below some threshold value. The percentage varying with threshold value can be viewed as a cumulative distribution. Figures 3c and 3f present the cumulative distributions of the error bounds. It can be seen that most of the state space can be guaranteed with much lower error bounds, with only a small percentage of the regions having larger guarantees. This is especially the case for the offset measurement: 99% of the state space is guaranteed to have error less than 2.65 (3.3% of the measurement range), while the global error bound is 12.66 (15.8%).

A key question for the error bounds is how well they reflect the actual maximum error made by the neural network. To study the tightness of the error bounds, we compute empirical estimates of the maximum errors for each  $S_i$ , denoted as  $\bar{e}_\delta^i$  and  $\bar{e}_\theta^i$ . To do this, we sample multiple  $(\delta, \theta)$  within each cell  $S_i$  and generate input images, then take the maximum over the errors of these points as the empirical estimate of the maximum error for  $S_i$ . The sample points are drawn on a sub-grid within each cell, with sampling spacing 0.05. Notice that this estimate is a lower bound on the maximum error for  $S_i$ . This provides a reference for evaluating the tightness of the error upper bounds we get from *Tiler*.

We take the maximum of  $\bar{e}_\delta^i$ 's and  $\bar{e}_\theta^i$ 's to get a lower bound estimate of the global maximum error. The lower bound estimate of the global maximum error for  $\delta$  is 9.12 (11.4% of the measurement range); for  $\theta$  is  $4.08^\circ$  (3.4% of the measurement range). We can see that the error bounds that *Tiler* delivers are close to the lower bound estimates derived from the observed errors that the network exhibits for specific inputs.

Having visualized the heatmaps for the bounds  $e_\delta^i$  and  $e_\theta^i$ , we subtract from them the error estimates  $\bar{e}_\delta^i$  and  $\bar{e}_\theta^i$  and plot the heatmaps for the resulting gaps in Figures 3b and 3e. We can see that most of the regions that have large error bounds are due to the fact that the network itself has large errors there. By computing the cumulative distributions of these gaps between bounds and estimates, we found that for angle measurement, 99% of the state space has error gap below  $1.9^\circ$  (1.6% of measurement range); and for offset measurement, 99% of the state space has error gap below 1.41 length units (1.8%). The gaps indicate the maximum possible improvements on the error bounds.

**Contributing factors to the gap:** There are two main contributing factors to the gap between the bound from *Tiler* and the actual maximum error. First is the systematic error introduced in the way



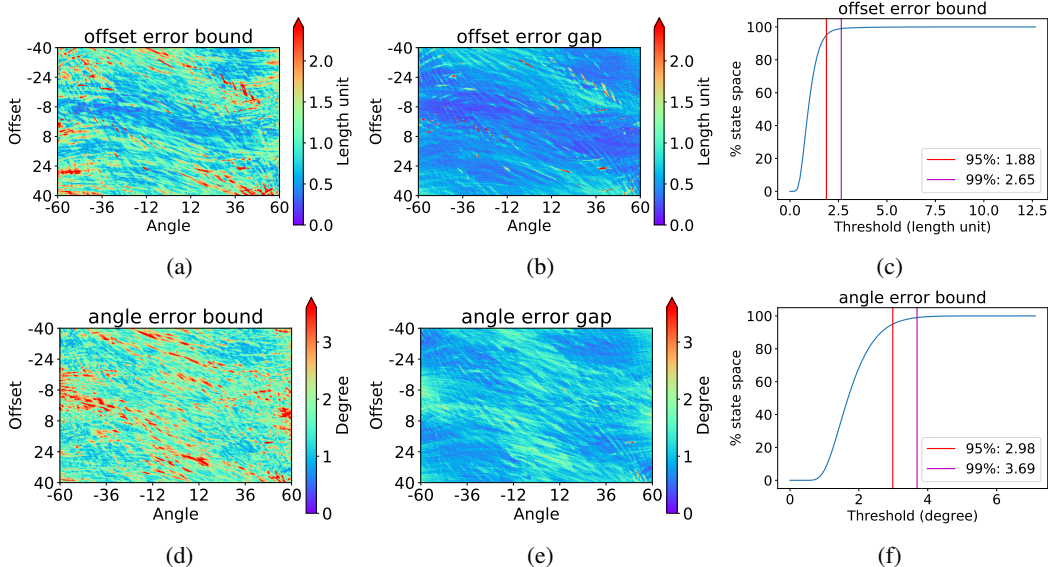


Figure 3: (a,d) Heatmaps of the upper bounds on the maximum error of each tile over the offset-angle space. (b,e) Corresponding heatmaps after subtracting empirical estimates of the actual maximum error. (c, f) Percentage of the state space with error upper bounds below some threshold value (cumulative distribution).

*Tiler* computes the error bound. *Tiler* takes the maximum distance between the range of possible ground truths and the range of possible network outputs as the bound. For a perfect network, this still gives a bound equal to the range of ground truth, instead of zero. The second factor is the extra space included in the box  $\mathcal{B}_i$  that is not on the tile  $\mathcal{X}_i$ . This results in a larger range on network output being used for calculating error bound, which in turn makes the error bound itself larger.

**Effect of tile size:** Both of the factors described above are affected by the tile size. We run *Tiler* with a sequence of cell sizes (0.05, 0.1, 0.2, 0.4, 0.8) for the  $(\delta, \theta)$  grid. Figure 4a shows how the 99 percentiles of the error upper bounds and the gap between error bounds and estimates vary with cell size. As tile size gets finer, *Tiler* provides better error bounds, and the tightness of bounds improves.

As another perspective, consider the case where we only trust the network when the error is less than some threshold. Figure 4b shows how the percentage of the state space where the network is proved to be trustworthy varies with cell size, given the required accuracy being 3% of the measurement range. It can be seen that with finer tile sizes, *Tiler* is able to prove larger trusted region.

These results show that we can get better error bounds with finer tile sizes. But this improvement might be at the cost of time: reducing tile sizes also increases the total number of tiles and the number of optimization problems to solve. Figure 4c shows how the total solving time varies with cell size. For cell sizes smaller than 0.2, the trend can be explained by the above argument. For cell sizes larger than 0.2, total solving time increases with cell size instead. The reason for this is that each optimization problem becomes harder to solve as the tile becomes large. Specifically, the approach we adopt [21] relies on the presolving on ReLU stability to improve speed. The number of unstable ReLUs will increase drastically as the cell size becomes large, which makes the solving slower.

## 6 Discussion

The techniques presented in this paper work with specifications provided by the combination of a state space of the world and an observation process that converts states into neural network inputs. Results from the case study highlight how well the approach works for a state space characterized by two attributes ( $\delta$  and  $\theta$ ) and a camera imaging observation process. We anticipate that the technique will also work well for other problems that have a low dimensional state space with a tractable tiling and an observation process that can be precisely modelled.

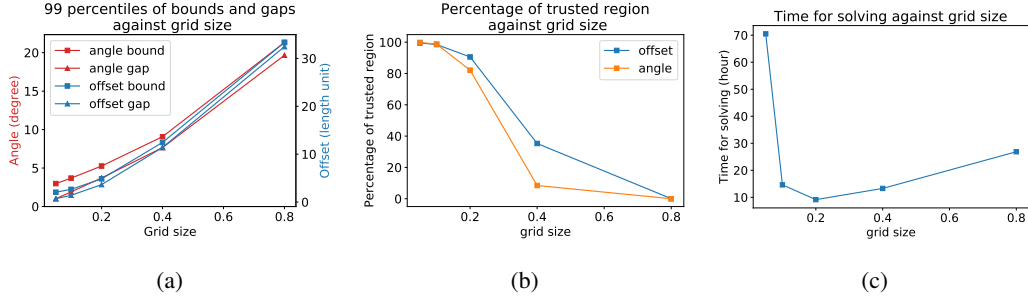


Figure 4: Effect of cell size on bound quality and solving time. (a) plots the 99 percentiles of the error upper bounds and the gaps between upper and lower bounds against cell size. (b) plots the percentage of the state space that is proved to be trustworthy (error less than 3% of measurement range) against cell size. (c) shows how the total solving time varies with cell size.

*Tiler* generalizes to cases where alternative methods exist for characterizing the feasible input space and the ground truth: we express the sufficient conditions (Condition 4.1 to 4.4) for soundness independent of the state space and the observation process. *Tiler* can therefore be applied and give sound correctness guarantees whenever there exist methods that can produce tiles, ground truth bounds, and bounding boxes that satisfy these conditions.

A final question is whether it is possible to determine whether an arbitrary input  $x \in X$  is feasible (i.e., whether  $x \in \tilde{X}$ ) and therefore whether the neural network is known to compute a correct output  $y$  for  $x$ . In general, we expect the answer to this question to depend on the precise characteristics of the specific problem, its state space, and the observation process. In particular, we are not aware of any computationally tractable method for determining if an input  $x$  is feasible for the problem in our case study. However, we anticipate that it will often be straightforward to determine if an arbitrary input  $x$  is contained in some bounding box  $B_i$ . In our case study, because we use bounding boxes defined by the  $l_\infty$  norm, it is straightforward to search the bounding boxes  $\{B_i\}$  and determine if  $x$  is contained in one of the bounding boxes. If so, the technique guarantees that there is an input  $x'$  close to  $x$  (i.e.,  $x$  and  $x'$  are both within the same bounding box  $B_i$ ) for which 1) the neural network computes an output  $y'$  that is correct up to the defined tolerance and 2) the output  $y'$  is close to the output  $y$  for  $x$  (i.e.,  $y'$  and  $y$  are both within the network output bound  $(l'_i, u'_i)$  for  $B_i$ ).

## Acknowledgements

We thank Vincent Tjeng for help on the MIPVerify software package. We thank Jie Xu for helpful discussions on the graphics process. We thank Aleksander Madry and Dimitris Tsipras for useful discussions on verifying robustness of neural networks. We thank Dimitris Tsipras for helpful feedback on an earlier draft of this paper. We thank Dragos Margineantu, Charles Erignac, Tyler Staudinger, Jeffery Saunders, and Craig Bonnoit for inspirational discussions on various aspect of machine learning.

## References

- [1] Osbert Bastani, Yani Ioannou, Leonidas Lampropoulos, Dimitrios Vytiniotis, Aditya V. Nori, and Antonio Criminisi. 2016. Measuring Neural Net Robustness with Constraints. In *Proceedings of the 30th International Conference on Neural Information Processing Systems (NIPS'16)*. Curran Associates Inc., USA, 2621–2629. <http://dl.acm.org/citation.cfm?id=3157382.3157391>
- [2] Chih-Hong Cheng, Georg Nührenberg, and Harald Ruess. 2017. Maximum Resilience of Artificial Neural Networks. In *ATVA*.
- [3] Souradeep Dutta, Susmit Jha, Sriram Sankaranarayanan, and Ashish Tiwari. 2018. Learning and Verification of Feedback Control Systems using Feedforward Neural Networks. *IFAC-PapersOnLine* 51, 16 (2018), 151 – 156. <https://doi.org/10.1016/j.ifacol.2018.08.026> 6th IFAC Conference on Analysis and Design of Hybrid Systems ADHS 2018.

- [4] Krishnamurthy Dvijotham, Robert Stanforth, Sven Gowal, Timothy Mann, and Pushmeet Kohli. 2018. A dual approach to scalable verification of deep networks. In *Proceedings of the Thirty-Fourth Conference Annual Conference on Uncertainty in Artificial Intelligence (UAI-18)*. AUA Press, Corvallis, Oregon, 162–171.
- [5] Rüdiger Ehlers. 2017. Formal Verification of Piece-Wise Linear Feed-Forward Neural Networks. *CoRR* abs/1705.01320 (2017). arXiv:1705.01320 <http://arxiv.org/abs/1705.01320>
- [6] T. Gehr, M. Mirman, D. Drachler-Cohen, P. Tsankov, S. Chaudhuri, and M. Vechev. 2018. AI2: Safety and Robustness Certification of Neural Networks with Abstract Interpretation. In *2018 IEEE Symposium on Security and Privacy (SP)*, 3–18. <https://doi.org/10.1109/SP.2018.00058>
- [7] Xiaowei Huang, Marta Kwiatkowska, Sen Wang, and Min Wu. 2017. Safety Verification of Deep Neural Networks. In *Computer Aided Verification*, Rupak Majumdar and Viktor Kunčák (Eds.). Springer International Publishing, Cham, 3–29.
- [8] Guy Katz, Clark Barrett, David L. Dill, Kyle Julian, and Mykel J. Kochenderfer. 2017. Reluplex: An Efficient SMT Solver for Verifying Deep Neural Networks. In *Computer Aided Verification*. Springer International Publishing, 97–117. [https://doi.org/10.1007/978-3-319-63387-9\\_5](https://doi.org/10.1007/978-3-319-63387-9_5)
- [9] Hayhurst Kelly J., Veerhusen Dan S., Chilenski John J., and Rierson Leanna K. 2001. *A Practical Tutorial on Modified Condition/Decision Coverage*. Technical Report.
- [10] Diederik P. Kingma and Jimmy Ba. 2014. Adam: A Method for Stochastic Optimization. *CoRR* abs/1412.6980 (2014). <http://arxiv.org/abs/1412.6980>
- [11] Changliu Liu, Tomer Arnon, Christopher Lazarus, Clark Barrett, and Mykel J. Kochenderfer. 2019. Algorithms for Verifying Deep Neural Networks. *CoRR* abs/1903.06758 (2019). arXiv:1903.06758 <http://arxiv.org/abs/1903.06758>
- [12] Alessio Lomuscio and Lalit Maganti. 2017. An approach to reachability analysis for feed-forward ReLU neural networks. *CoRR* abs/1706.07351 (2017). arXiv:1706.07351 <http://arxiv.org/abs/1706.07351>
- [13] Lei Ma, Felix Juefei-Xu, Jiyuan Sun, Chunyang Chen, Ting Su, Fuyuan Zhang, Minhui Xue, Bo Li, Li Li, Yang Liu, Jianjun Zhao, and Yadong Wang. 2018. DeepGauge: Comprehensive and Multi-Granularity Testing Criteria for Gauging the Robustness of Deep Learning Systems. *CoRR* abs/1803.07519 (2018). arXiv:1803.07519 <http://arxiv.org/abs/1803.07519>
- [14] Augustus Odena and Ian J. Goodfellow. 2018. TensorFuzz: Debugging Neural Networks with Coverage-Guided Fuzzing. *CoRR* abs/1807.10875 (2018).
- [15] Nicolas Papernot, Patrick D. McDaniel, Somesh Jha, Matt Fredrikson, Z. Berkay Celik, and Ananthram Swami. 2016. The Limitations of Deep Learning in Adversarial Settings. *2016 IEEE European Symposium on Security and Privacy (EuroS&P)* (2016), 372–387.
- [16] Kexin Pei, Yinzhi Cao, Junfeng Yang, and Suman Jana. 2017. DeepXplore: Automated Whitebox Testing of Deep Learning Systems. In *Proceedings of the 26th Symposium on Operating Systems Principles (SOSP '17)*. ACM, New York, NY, USA, 1–18. <https://doi.org/10.1145/3132747.3132785>
- [17] Aditi Raghunathan, Jacob Steinhardt, and Percy Liang. 2018. Certified Defenses against Adversarial Examples. In *International Conference on Learning Representations*. <https://openreview.net/forum?id=Bys4ob-Rb>
- [18] Youcheng Sun, Xiaowei Huang, and Daniel Kroening. 2018. Testing Deep Neural Networks. *CoRR* abs/1803.04792 (2018). arXiv:1803.04792 <http://arxiv.org/abs/1803.04792>
- [19] Christian Szegedy, Wojciech Zaremba, Ilya Sutskever, Joan Bruna, Dumitru Erhan, Ian J. Goodfellow, and Rob Fergus. 2014. Intriguing properties of neural networks. *CoRR* abs/1312.6199 (2014).

- [20] Yuchi Tian, Kexin Pei, Suman Jana, and Baishakhi Ray. 2018. DeepTest: Automated Testing of Deep-neural-network-driven Autonomous Cars. In *Proceedings of the 40th International Conference on Software Engineering (ICSE '18)*. ACM, New York, NY, USA, 303–314. <https://doi.org/10.1145/3180155.3180220>
- [21] Vincent Tjeng, Kai Y. Xiao, and Russ Tedrake. 2019. Evaluating Robustness of Neural Networks with Mixed Integer Programming. In *International Conference on Learning Representations*. <https://openreview.net/forum?id=HyGIIdiRqtm>
- [22] Tsui-Wei Weng, Huan Zhang, Hongge Chen, Zhao Song, Cho-Jui Hsieh, Duane Boning, Inderjit S. Dhillon, and Luca Daniel. 2018. Towards Fast Computation of Certified Robustness for ReLU Networks. In *International Conference on Machine Learning (ICML)*.
- [23] Eric Wong and Zico Kolter. 2018. Provable Defenses against Adversarial Examples via the Convex Outer Adversarial Polytope. In *Proceedings of the 35th International Conference on Machine Learning (Proceedings of Machine Learning Research)*, Jennifer Dy and Andreas Krause (Eds.), Vol. 80. PMLR, Stockholmsmässan, Stockholm Sweden, 5286–5295. <http://proceedings.mlr.press/v80/wong18a.html>
- [24] Eric Wong, Frank Schmidt, Jan Hendrik Metzen, and J. Zico Kolter. 2018. Scaling provable adversarial defenses. In *Advances in Neural Information Processing Systems 31*, S. Bengio, H. Wallach, H. Larochelle, K. Grauman, N. Cesa-Bianchi, and R. Garnett (Eds.). Curran Associates, Inc., 8400–8409. <http://papers.nips.cc/paper/8060-scaling-provable-adversarial-defenses.pdf>
- [25] Weiming Xiang, Hoang-Dung Tran, and Taylor T. Johnson. 2017. Reachable Set Computation and Safety Verification for Neural Networks with ReLU Activations. *CoRR* abs/1712.08163 (2017). arXiv:1712.08163 <http://arxiv.org/abs/1712.08163>
- [26] W. Xiang, H. Tran, J. A. Rosenfeld, and T. T. Johnson. 2018. Reachable Set Estimation and Safety Verification for Piecewise Linear Systems with Neural Network Controllers. In *2018 Annual American Control Conference (ACC)*. 1574–1579. <https://doi.org/10.23919/ACC.2018.8431048>
- [27] Weiming Xiang, Hoang-Dung Tran, and Taylor T. Johnson. 2018. Output Reachable Set Estimation and Verification for Multi-Layer Neural Networks. *IEEE Transactions on Neural Networks and Learning Systems (TNNLS)* (March 2018). <https://doi.org/10.1109/TNNLS.2018.2808470>

## Appendices

### A Proofs for Theorem 1 and 2

**Theorem 1** (Local error bound for regression). *Given that Condition 4.1, 4.2(a), 4.3, and 4.4(a) are satisfied, then  $\forall x \in \tilde{\mathcal{X}}$ ,  $e(x) \leq e_{\text{local}}(x)$ , where  $e(x)$  is defined in Equation 2 and  $e_{\text{local}}(x)$  is computed from Equation 3 and 5.*

*Proof.* For any  $x \in \tilde{\mathcal{X}}$ , we have

$$\begin{aligned} e(x) &= \max_{y \in \hat{f}(x)} d(f(x), y) \\ &= \max_{y \in \hat{f}(x)} |f(x) - y| \\ &= \max_{y \in \hat{f}(x)} \{\max(f(x) - y, y - f(x))\} \end{aligned}$$

Condition 4.1 and 4.2(a) guarantees that for any  $x \in \tilde{\mathcal{X}}$  and  $y \in \hat{f}(x)$ , we can find a tile  $\mathcal{X}_i$  such that  $x \in \mathcal{X}_i$  and  $l_i \leq y \leq u_i$ . Let  $t(y, x)$  be a function that gives such a tile  $\mathcal{X}_{t(y, x)}$  for a given  $x$  and  $y \in \hat{f}(x)$ . Then

$$e(x) \leq \max_{y \in \hat{f}(x)} \{\max(f(x) - l_{t(y, x)}, u_{t(y, x)} - f(x))\}.$$

Since  $x \in \mathcal{X}_{t(y, x)}$  and  $\mathcal{X}_{t(y, x)} \subseteq \mathcal{B}_{t(y, x)}$  (Condition 4.3),  $x \in \mathcal{B}_{t(y, x)}$ . By Condition 4.4(a),

$$l'_{t(y, x)} \leq f(x) \leq u'_{t(y, x)}, \forall y \in \hat{f}(x).$$

This gives

$$\begin{aligned} e(x) &\leq \max_{y \in \hat{f}(x)} \{\max(u'_{t(y, x)} - l_{t(y, x)}, u_{t(y, x)} - l'_{t(y, x)})\} \\ &= \max_{y \in \hat{f}(x)} e_{t(y, x)} \end{aligned}$$

Since  $x \in \mathcal{B}_{t(y, x)}$  for all  $y \in \hat{f}(x)$ , we have  $\{t(y, x) | y \in \hat{f}(x)\} \subseteq \{i | x \in \mathcal{B}_i\}$ , which gives

$$\begin{aligned} e(x) &\leq \max_{\{t(y, x) | y \in \hat{f}(x)\}} e_{t(y, x)} \\ &\leq \max_{\{i | x \in \mathcal{B}_i\}} e_i \\ &= e_{\text{local}}(x) \end{aligned}$$

□

**Theorem 2** (Global error bound for regression). *Given that Condition 4.1, 4.2(a), 4.3, and 4.4(a) are satisfied, then  $\forall x \in \tilde{\mathcal{X}}$ ,  $e(x) \leq e_{\text{global}}$ , where  $e(x)$  is defined in Equation 2 and  $e_{\text{global}}$  is computed from Equation 3 and 4.*

*Proof.* By Theorem 1, we have  $\forall x \in \tilde{\mathcal{X}}$ ,

$$\begin{aligned} e(x) &\leq \max_{\{i | x \in \mathcal{B}_i\}} e_i \\ &\leq \max_i e_i \\ &= e_{\text{global}} \end{aligned}$$

□

## B Classification

We present here the algorithm of *Tiler* for classification settings.

**Step 1** (tiling the space) is the same as regression.

**Step 2:** For each  $\mathcal{S}_i$ , compute the ground truth bound as a set  $\mathcal{C}_i \subseteq \mathcal{Y}$ , such that  $\forall s \in \mathcal{S}_i, \lambda(s) \in \mathcal{C}_i$ .

The bounds computed this way satisfy the following condition:

*Condition 4.2(b).* For any  $x \in \tilde{\mathcal{X}}, \forall y \in \hat{f}(x), \exists \mathcal{X}_i$  such that  $x \in \mathcal{X}_i$  and  $y \in \mathcal{C}_i$ .

The idea behind *Condition 4.2(b)* is the same as that of *Condition 4.2(a)*, but formulated for discrete  $y$ .

**Step 3** (compute bounding box for each input tile) is the same as regression.

The next step is to solve the network output range. Suppose the quantity of interest has  $K$  possible classes. Then the output layer of the neural network is typically a softmax layer with  $K$  output nodes. Denote the  $k$ -th output score before softmax as  $o_k(x)$ . We use the solver to solve the range of each output score:

**Step 4:** Given  $f$  and each  $\mathcal{B}_i$ , use appropriate solver to solve the range of each output score  $(l_i^{(k)}, u_i^{(k)})$  for  $k = 1, \dots, K$ .

The bounds  $\{(l_i^{(k)}, u_i^{(k)})\}$  need to satisfy:

*Condition 4.4(b)*  $\forall x \in \mathcal{B}_i, \forall k \in \{1, \dots, K\}, l_i^{(k)} \leq o_k(x) \leq u_i^{(k)}$ .

**Step 5:** For each tile, compute an error bound  $e_i$ , using the bound on ground truth  $\mathcal{C}_i$  and the bound on network output  $\{(l_i^{(k)}, u_i^{(k)})\}_{k=1, \dots, K}$ :

$$e_i = 0 \text{ if and only if the following conditions hold:} \quad (7)$$

1.  $\mathcal{C}_i$  only contains one element, and
2.  $l_i^{(y_{\mathcal{C}_i})} > u_i^{(k)}$  for all  $k \neq y_{\mathcal{C}_i}$ , where  $y_{\mathcal{C}_i}$  is the class index of the only element in  $\mathcal{C}_i$ .

Otherwise,  $e_i = 1$ . We can then compute the global and local error bounds using Equation 4 and 5, same as in the regression case. The error bounds for classification will be binary, with 0 meaning the network is guaranteed to be correct, and 1 meaning no guarantee.

**Theorem 3** (Local error bound for classification). *Given that Condition 4.1, 4.2(b), 4.3, and 4.4(b) are satisfied, then  $\forall x \in \tilde{\mathcal{X}}, e(x) \leq e_{\text{local}}(x)$ , where  $e(x)$  is defined in Equation 2 and  $e_{\text{local}}(x)$  is computed from Equation 7 and 5. Equivalently, when  $e_{\text{local}}(x) = 0$ , the network prediction is guaranteed to be correct at  $x$ .*

*Proof.* We aim to prove that  $\forall x \in \tilde{\mathcal{X}}$ , if  $e_{\text{local}}(x) = 0$ , then  $f(x) = \hat{f}(x)$ . First, according to the definition of  $e_{\text{local}}(x)$ ,  $e_{\text{local}}(x) = 0$  implies  $e_i = 0$  for all  $i \in \{i | x \in \mathcal{B}_i\}$ . Arbitrarily pick a  $p \in \{i | x \in \mathcal{B}_i\}$ , we have  $e_p = 0$ . According to Equation 7,  $\mathcal{C}_p$  only contains one element with class index  $y_{\mathcal{C}_p}$ , and  $l_p^{(y_{\mathcal{C}_p})} > u_p^{(k)}$  for all  $k \neq y_{\mathcal{C}_p}$ . Since  $x \in \mathcal{B}_p$ , Condition 4.4(b) gives:

$$o_{y_{\mathcal{C}_p}}(x) \geq l_p^{(y_{\mathcal{C}_p})} > u_p^{(k)} \geq o_k(x)$$

for all  $k \neq y_{\mathcal{C}_p}$ . This gives  $f(x) = y_{\mathcal{C}_p}$ . For any  $q \in \{i | x \in \mathcal{B}_i, i \neq p\}$ , we can similarly derive  $f(x) = y_{\mathcal{C}_q}$ . Therefore, we must have  $y_{\mathcal{C}_q} = y_{\mathcal{C}_p}$  for all  $q \in \{i | x \in \mathcal{B}_i, i \neq p\}$ , otherwise there will be a contradiction. In another word, we have

$$\bigcup_{\{i | x \in \mathcal{B}_i\}} \mathcal{C}_i = \{y_{\mathcal{C}_p}\}$$

Now, according to Condition 4.2(b),  $\forall y \in \hat{f}(x), \exists \mathcal{X}_i$  such that  $x \in \mathcal{X}_i$  and  $y \in \mathcal{C}_i$ . Rewriting this condition, we get

$$\forall y \in \hat{f}(x), y \in \bigcup_{\{i | x \in \mathcal{X}_i\}} \mathcal{C}_i$$

which also means  $\hat{f}(x) \subseteq \bigcup_{\{i|x \in \mathcal{X}_i\}} \mathcal{C}_i$ . But  $\{i|x \in \mathcal{X}_i\} \subseteq \{i|x \in \mathcal{B}_i\}$  (Condition 4.3), which gives

$$\hat{f}(x) \subseteq \bigcup_{\{i|x \in \mathcal{X}_i\}} \mathcal{C}_i \subseteq \bigcup_{\{i|x \in \mathcal{B}_i\}} \mathcal{C}_i = \{y_{\mathcal{C}_p}\}.$$

Since  $\hat{f}(x)$  is not empty, we have  $\hat{f}(x) = \{y_{\mathcal{C}_p}\} = f(x)$ .  $\square$

**Theorem 4** (Global error bound for classification). *Given that Condition 4.1, 4.2(b), 4.3, and 4.4(b) are satisfied, then if  $e_{\text{global}} = 0$ , the network prediction is guaranteed to be correct for all  $x \in \tilde{\mathcal{X}}$ .  $e_{\text{global}}$  is computed from Equation 7 and 4.*

*Proof.* We aim to prove that if  $e_{\text{global}} = 0$ , then  $\forall x \in \tilde{\mathcal{X}}, f(x) = \hat{f}(x)$ . According to Equation 4,  $e_{\text{global}} = 0$  means  $e_i = 0$  for all  $i$ . Then  $\forall x \in \tilde{\mathcal{X}}, e_{\text{local}}(x) = 0$ , which by Theorem 3 indicates that  $f(x) = \hat{f}(x)$ .  $\square$

Algorithm 2 formally presents the *Tiler* algorithm for classification.

---

**Algorithm 2** Tiler (for classification)

---

**Input:**  $\mathcal{S}, g, \lambda, f$   
**Output:**  $e_{\text{global}}, \{e_i\}, \{\mathcal{B}_i\}$

- 1: **procedure** TILER( $\mathcal{S}, g, \lambda, f$ )
- 2:    $\{\mathcal{S}_i\} \leftarrow \text{DIVIDESTATESPACE}(\mathcal{S})$   $\triangleright$  Step 1
- 3:   **for each**  $\mathcal{S}_i$  **do**
- 4:      $\mathcal{C}_i \leftarrow \text{GETGROUNDTRUTHBOUND}(\mathcal{S}_i, \lambda)$   $\triangleright$  Step 2
- 5:      $\mathcal{B}_i \leftarrow \text{GETBOUNDINGBOX}(\mathcal{S}_i, g)$   $\triangleright$  Step 3
- 6:      $\{l_i^{(k)}, u_i^{(k)}\}_{k=1, \dots, K} \leftarrow \text{SOLVER}(f, \mathcal{B}_i)$   $\triangleright$  Step 4
- 7:      $e_i \leftarrow \text{GETERRORBOUND}(\mathcal{C}_i, \{l_i^{(k)}, u_i^{(k)}\}_{k=1, \dots, K})$   $\triangleright$  Step 5, Equation 7
- 8:   **end for**
- 9:    $e_{\text{global}} \leftarrow \max(\{e_i\})$   $\triangleright$  Step 5
- 10: **return**  $e_{\text{global}}, \{e_i\}, \{\mathcal{B}_i\}$   $\triangleright \{e_i\}, \{\mathcal{B}_i\}$  can be used later to compute  $e_{\text{local}}(x)$
- 11: **end procedure**

---

## C Additional Training Details

This section presents the additional details of the training of the neural network in the case study. We use Adam optimizer with learning rate 0.01. We use early stopping based on the loss on the validation set: we terminate training if the validation performance does not improve in 5 consecutive epochs. This results in the training terminated at 21 epochs. We take the model from the epoch that has the lowest loss on the validation set.